Sedimentary Geology 429 (2022) 106073

Contents lists available at ScienceDirect

Sedimentary Geology

journal homepage: www.elsevier.com/locate/sedgeo

Origin of hematite in the Middle Cretaceous red chalks on the eastern coast of England

Tao Zhang [a,b], Xiuming Liu [a,b,c,*], Mingming Ma [b,d], Bin Lü [b,d], Xuegang Mao [b,d], Jiasheng Chen [b,d], Gengyu Liu [a,e], Yang Tang [f]

[a] College of Geographical Sciences, Fujian Normal University, Fuzhou 35007, China
[b] Key Laboratory for Subtropical Mountain Ecology, Fujian Normal University, Fuzhou 35007, China
[c] Department of Environment and Geography, Macquarie University, Sydney, NSW 2109, Australia
[d] Institute of Geography, Fujian Normal University, Fuzhou 350007, China
[e] Fuzhou Investigation and Surveying Institute, Fuzhou, Fujian 350108, China
[f] State Key Laboratory of Environmental Geochemistry, Institute of Geochemistry, Chinese Academy of Sciences, Guiyang 550081, China

ARTICLE INFO

Article history:
Received 21 September 2021
Received in revised form 16 December 2021
Accepted 20 December 2021
Available online 28 December 2021

Editor: Dr. Catherine Chagué

Keywords:
Red chalk
Fe isotope
Rare earth elements
Pedogenic origin
Middle Cretaceous
England

ABSTRACT

Chalks are generally believed to have formed in shallow marine environments. However, the consensus on sources of Fe and origin of hematite in red chalks remains elusive. To better understand the origin of hematite in the Middle Cretaceous red chalks on the eastern coast of England, the evidence has been gathered through diffuse reflection, trace element and iron isotope analysis and combining with the lithologic and stratigraphic characteristics. Rare earth element (REE) patterns exhibit upper-continental-crust-like signatures such as enrichment in light REEs and depletion in heavy REEs. The Fe isotopic composition of the red chalk is typically heavier than that of igneous rocks (except for one sample) and shows negative Eu anomalies ($Eu/Eu^* = 0.58–0.73$), which indicates that the hematite in the red chalk is not of microbial or hydrothermal, but of sedimentary origin. At the same time, the analysis of trace elements suggests that the felsic rocks and sedimentary derivatives are the source of non-carbonate components in the red chalks. The pedogenic features such as mudcracks, secondary white chalks, and calcareous nodules appear in the red chalks, as documented through the field stratigraphic observations. Based on the above evidence and the sedimentary environment of the overlying and underlying layers, it is inferred that the red chalk was deposited in the supratidal environment that had undergone some degree of desiccation and pedogenic modification.

1. Introduction

The color of sediments serves as the basis for various geological interpretations, such as reconstruction of paleoclimates, redox conditions, and the genesis of clastic materials (Cai et al., 2012). It is generally believed that the red or black color of the sediment represents the presence of an oxidizing or reducing environment during deposition, respectively. Chalk is a white, gray, or red limestone consisting of over 98% calcium carbonate mainly from coccoliths, and few microfossils such as bryozoans, echinoids and ostracods, which is the characteristic deposit of the Cretaceous in northwestern France, northeastern, southern, and out to the eastern England (Hancock, 1975; Aliyu, 2016). Recent studies have shown that the Chalk was deposited in environments ranging from neritic to pelagic settings based on fossils and sedimentary structures during the global transgression of the Cretaceous (Hancock, 1975; Surlyk, 1997; Mortimore, 2001; Wray and Gale, 2006; Lasseur et al., 2009; Giorgioni et al., 2015; Belghouthi et al., 2019). The presence of gypsum in the chalk in the Upper Cretaceous rocks of the Voronezh Anteclise indicates a lagoonal environment in an arid climate during that period (Zhabin et al., 2018), which provides a possible evidence for chalk deposition in an oxidized environment.

Oxidation conditions are one of the decisive factors for the formation and preservation of hematite in red beds (X.M. Hu et al., 2012). The red beds have long been of interest to geologists because of their paleoenvironmental and paleoclimatic potential. The main mineral carrier of red color is hematite; consequently, the formation of red beds is attributed to hematite enrichment. There are five main hypotheses to explain the origin of the hematite pigment: (1) a detrital origin in which hematite was derived from continental weathering during sedimentation (Von Houten, 1961; Zhang, 2015); (2) a diagenetic origin assumed that hematite formed by dehydration of goethite after deposition (Walker, 1967; Retallack, 2001); (3) a hydrothermal origin

* Corresponding author at: College of Geographical Sciences, Fujian Normal University, Fuzhou 35007, China.
E-mail address: xliu@fjnu.edu.cn (X. Liu).

https://doi.org/10.1016/j.sedgeo.2021.106073
0037-0738/

of iron ions that were derived from mantle and deposited in the sediments with magmatic hydrothermal fluids (Frei and Polat, 2007; Li et al., 2008; Wang et al., 2017); (4) a microbial origin was proposed for hematite pigment because of the fact that hematite can be formed by the mediation of iron-bacteria near the interface between water and sediment (Mamet and Préat, 2006; Préat et al., 2018); (5) a pedogenic origin was based on the formation of hematite in dry soils in a surface environment (Schaetzl and Anderson, 2005; Liu et al., 2014). In addition to the depositional mechanisms, Fe element in the red bed may be derived from continental weathering (Zhang, 2015) or hydrothermal eruption (Wang et al., 2017).

The occurrence of colored chalks ranging from red to pink or white is an enigmatic phenomenon of the Cretaceous in eastern England (Jeans et al., 2016). The origin of the hematitic pigment in the Hunstanton Red Chalk Formation of the Middle Cretaceous has been controversial for a long time. Three hypotheses for hematite in red chalks have been proposed in recent years: diagenetic origin (Jeans, 1973), volcanic or hydrothermal origin (Jeans et al., 2000, 2016) and microbial origin (Andrews et al., 2015). Taking the Hunstanton and Speeton sections from the east coast of England as the study object, the main purpose of this study is to assess the previous viewpoints on the origin of the red chalks by means of diffuse reflection, trace element and iron isotope analysis. On the basis of the above analysis and combining with the lithologic and stratigraphic characteristics, a pedogenic origin of red chalks is put forward. This signal can provide valuable information about pedogenic processes in karstic coastal environments and also provides evidence for the sedimentary environment of chalks.

2. Geological background

Chalk is found commonly in the east and south of England and spreads out to the northwestern France. Strips of red chalk between 1 and 24 m thick are particularly prominent on the east coast of England (Fig. 1a) (Price, 1998; Jeans et al., 2016). The strata reach from Albian to Cenomanian of the Middle Cretaceous in age and are well exposed (Owen, 1995; Hopson et al., 2008). The exposed strata comprise, in ascending order, the Carstone Formation, Hunstanton Red Chalk Formation and Ferriby Chalk Formation (Fig. 1b) (Owen, 1995; Price and Harwood, 2012).

The Carstone Formation is distributed in Cambridgeshire in southern England, where it is not seen at outcrop, and extends northward through Norfolk and is best exposed at Hunstanton. It is usually about 5 m thick, with a maximum thickness of 18.9 m at Hunstanton (Hopson et al., 2008). The typical lithology of the Carstone Formation

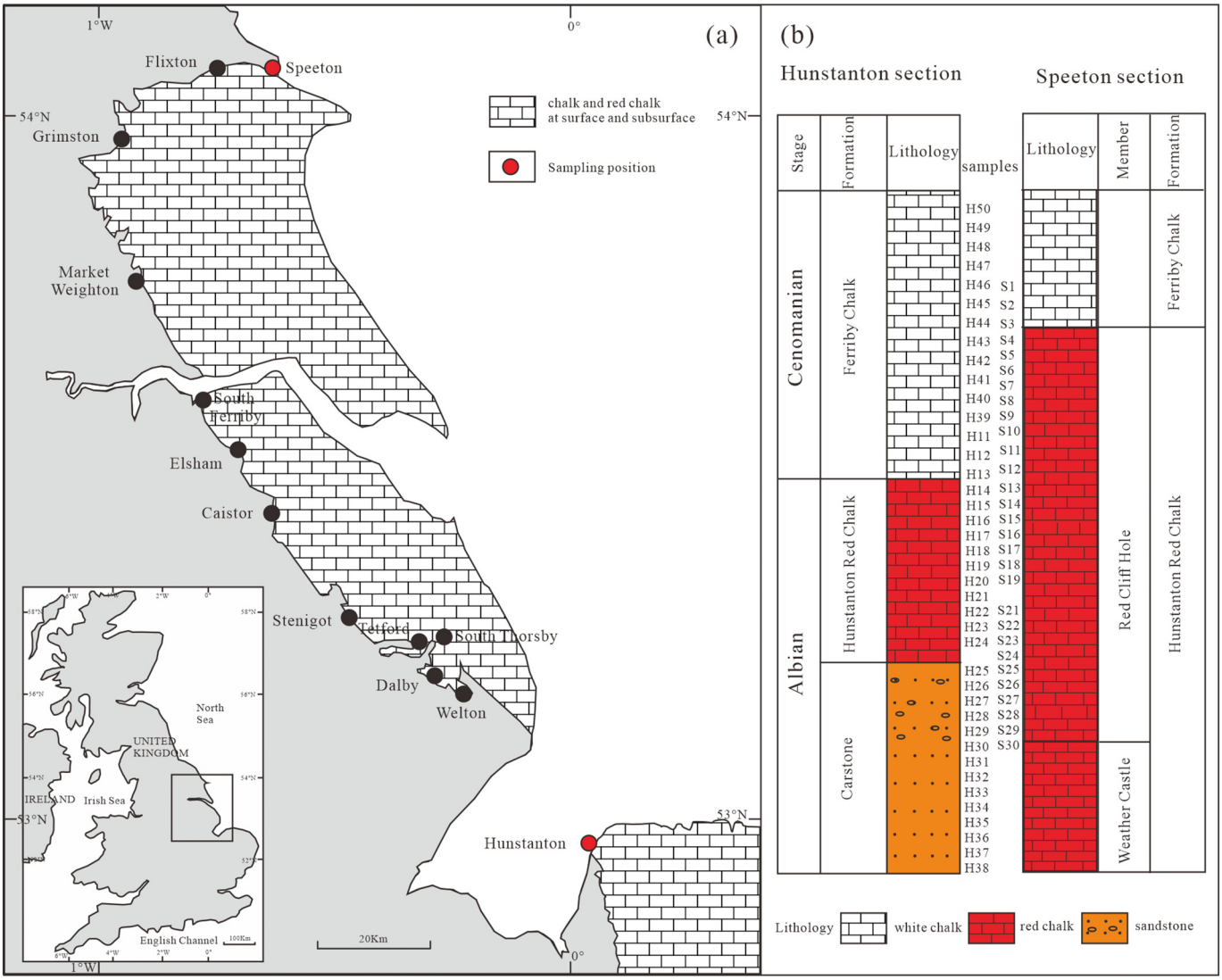

Fig. 1. (a) Distribution of chalk and red chalk at the surface and subsurface in eastern England (modified from references X.F. Hu et al., 2012; Price and Harwood, 2012; Jeans et al., 2016). The red chalk is restricted to the area between Hunstanton and Speeton. (b) Generalized stratigraphic column of the Hunstanton and Speeton sections from the Albian to Cenomanian stage of the Cretaceous with a notation of main lithologies (modified from references Mitchell, 1995; Price and Harwood, 2012).

is mainly medium- to coarse-grained brown sandstone with quartz pebbles in part and massive crossbedded (Owen, 1995; Hopson et al., 2008). The Hunstanton Red Chalk Formation is widespread in Yorkshire and Lincolnshire and extends southwards to the Hunstanton coast (Hopson et al., 2008). The thickness is usually 3 m in Lincolnshire and south Yorkshire, ~1 m and 24 m in the Hunstanton and Speeton sections, respectively (Mitchell, 1995; Hopson et al., 2008). The formation consists of pink to brick-red massive chalks with marly bands and an ammonite fauna, but locally white or gray due to secondary alteration (Owen, 1995; Hopson et al., 2008; Jeans et al., 2016). The age of the overlying Ferriby Formation ranges from 93.5 ± 0.8 Ma to 99.6 ± 0.9 Ma (Aliyu, 2016). The typical lithology of the Ferriby Chalk Formation is predominantly white chalk with abundant fragments of inoceramid bivalves (Owen, 1995; Price and Harwood, 2012).

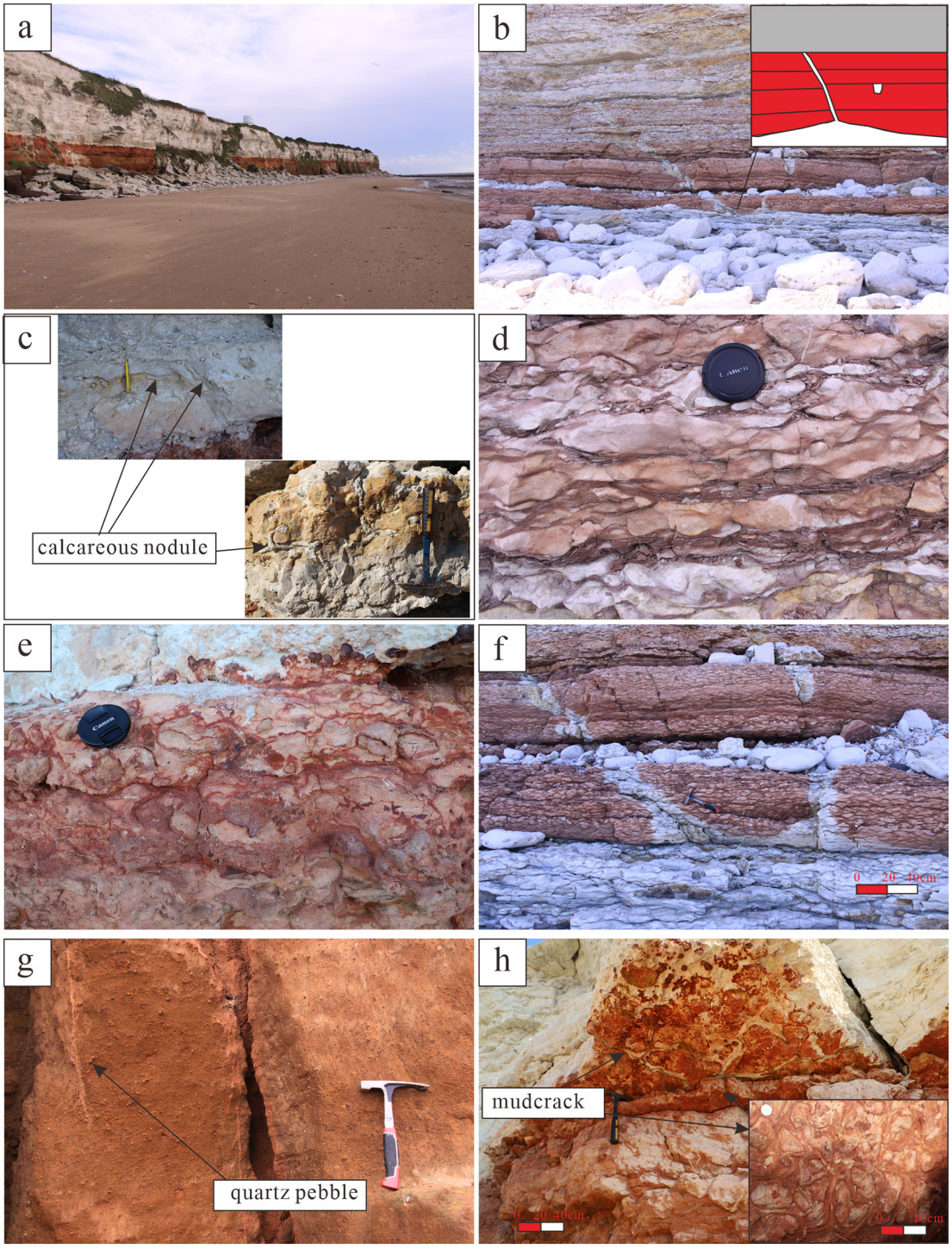

Fig. 2. (a) Panoramic view of the Hunstanton section. (b) The studied interval of the Speeton section and a sketch view of the secondary white chalks. (c) Various forms of calcareous nodules, including columnar, branching, or other irregular shapes, are found at the base of the white Ferriby Chalk Formation in the Hunstanton section. (d, e) The redder chalks are distributed in a reticulate form in the Hunstanton Red Chalk Formation. (f) Secondary white chalks in the Speeton section are formed at inclined or vertical fractures of the red chalk formation. (g) Brown pebbly sandstone of the Hunstanton section. (h) Mudcracks appeared on the top of the Hunstanton Red Chalk Formation in Hunstanton section.

3. Materials and methods

Samples for this study were collected from the Hunstanton and Speeton sections on the east coast of England, where red chalk is exposed (Fig. 1a). In total, 18 samples from the Ferriby Chalk Formation, 37 samples from the Hunstanton Red Chalk Formation and 14 samples from the Carstone Formation were analyzed for the present investigation (Fig. 1b). Eleven samples were collected from the Hunstanton Red Chalk formation in the Hunstanton section at 10 cm intervals. Other samples were collected at 20 cm intervals.

The samples were crushed to 200-mesh powders for diffuse reflectance spectroscopy, trace element, and Fe isotope analysis. The representative samples were selected and heated in a Muffle furnace for 2 h at 300 °C (Zhou et al., 2007). The diffuse reflectance spectroscopy of samples before and after heating was measured with a UV-2600 spectrophotometer (Shimadzu Instruments Manufacturing Co., Ltd.), with the measuring wavelength range of 400 to 700 nm in 1 nm steps. The characteristic peak of the first derivative could be used to identify minerals and estimate the relative contents of hematite and goethite.

Trace elemental analysis was performed on bulk dissolutions of aliquots of the pulverized samples on an X-Series II inductively coupled plasma mass spectrometer (ICP-MS). Approximately 40 mg of powered sample was dissolved using HF, HNO_3 and $HClO_4$ in Teflon. The uncertainty of trace-element analyses is less than 10%.

Fe isotopic analysis was performed on 6 and 8 representative red chalks from Hunstanton and Speeton sections, respectively. Firstly, the powder samples of the representative red chalks were digested with HF-HNO_3 and HCl-HNO_3 mixed acids. Secondly, anionic resin (AG1-X8, 200–400 mesh) was used for chemical purification of iron. Finally, Fe isotope compositions of the red chalks were measured using a Thermo Fisher Scientific Neptune Plus multiple collector ICP-MS in medium-resolution mode. The sample-standard-bracketing method with IRMM-524a as the process standard sample was used to correct instrument deviation in this experiment. Iron isotope results were expressed in standard delta notation in per mil (‰) as $\delta^{56}Fe$ relative to the process standard IRMM-524a:

$$\delta^{56}Fe\ (‰) = 1000 \times \left[\left({}^{56}Fe/{}^{54}Fe\right)_{sample} / \left({}^{56}Fe/{}^{54}Fe\right)_{IRMM-524a} \right]$$

The Fe isotope composition of the international whole-rock standards, BHVO-2 ($\delta^{56}Fe = 0.12 \pm 0.05‰$; n = 3, 2SD), measured in this study, was consistent with the recommended values (Craddock and Dauphas, 2011).

Fe isotopic analysis was carried out at the State Key Laboratory of Environmental Geochemistry, Institute of Geochemistry Chinese Academy of Sciences, Guiyang, China, and other measurements were conducted at the Key Laboratory for Subtropical Mountain Ecology, Fujian Normal University, Fuzhou, China.

4. Results

4.1. Field stratigraphic and petrographic observations

The Hunstanton section is characterized by three distinct parallel colored bands, consisting of brown sandstone, red chalk and white chalk (Fig. 2a) (Owen, 1995; Price and Harwood, 2012). The Carstone Formation contains large amounts of ~2- to 5-mm pebbles in brown

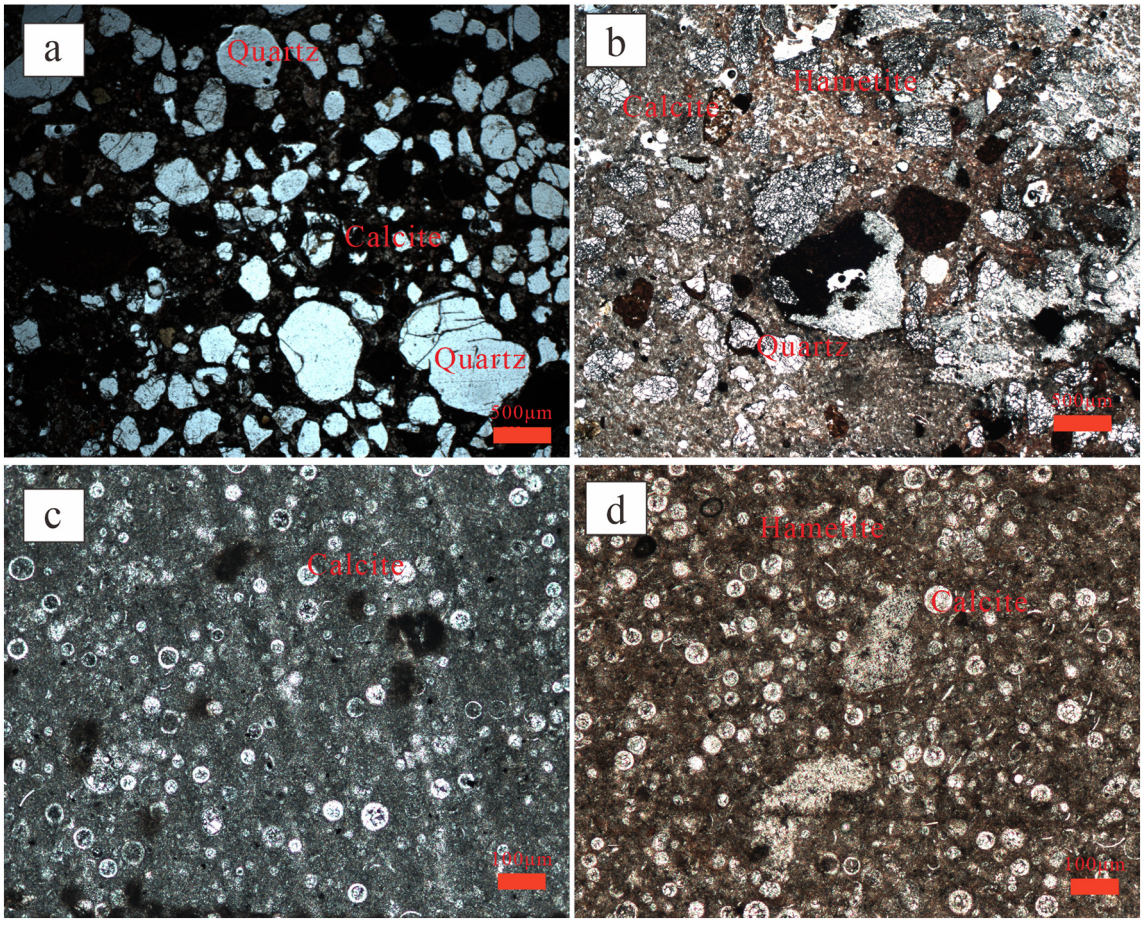

Fig. 3. The thin section characters of red chalks and secondary white chalks (c); (a, b) quartz particles of 50 μm to 1000 μm are cemented with calcite and hematite; (d) the red chalk is mainly composed of calcite and fine-grained hematite.

sandstone (Fig. 2g). There are also more quartz grains of 50 μm to 1000 μm in the red chalk at the bottom of the Hunstanton Red Chalk Formation (Fig. 3a). The red chalk is mainly composed of large amounts of calcite and small amounts of hematite (Fig. 2e; Fig. 3b). At the top of the Hunstanton Red Chalk Formation, the mudcracks of the red chalk are filled with either red or white chalk (Fig. 2h). Particularly prominent calcareous nodules are found in the Ferriby Chalk Formation, as well as in loess (Li et al., 2018) and paleosol (Guo et al., 2018; Menezes et al., 2021). Calcareous nodules of columnar, branching, or other irregular shapes are distributed in this formation (Fig. 2c). Hematite of the Hunstanton Red Chalk Formation is distributed in the chalk matrix with a reticulate form (Figs. 2d, e, 3b, d). Secondary white chalks in the Speeton section are formed at inclined or vertical fractures of the red chalk formation (Fig. 2b, f) due to the absence of hematite (Fig. 3c, d).

4.2. Diffuse reflectance spectroscopy

Diffuse reflectance spectroscopy was sensitive to changes in iron oxide content in sediments and could detect hematite and goethite as low as 0.01%, providing a rapid and effective method for the identification of hematite and goethite (Balsam et al., 2014). In general, in the first derivative curves of diffuse reflectance spectroscopy, the characteristic peak of hematite is between 555 and 575 nm. Goethite has two characteristic peaks, the main peak is at 535 nm and the secondary peak is at 435 nm. The higher the peak, the higher the relative content of hematite or goethite. Therefore, the value of first derivative from 565 nm and 435 nm was calculated to indicate the changes in the contents of hematite and goethite, respectively. Fig. 2 shows the first derivative curves of the diffuse reflectance spectroscopy of samples from the Hunstanton and Speeton sections before and after heating treatment. The results of diffuse reflectance spectroscopy can be divided into three groups (Fig. 4): the sandstones of the Carstone Formation in the Hunstanton section exhibit two peaks at approximately 435 and 535 nm in the first derivative spectral (FDV) patterns, and become a single peak at 570 nm after heating at 300 °C, indicating the presence of goethite only (Fig. 4a, c); the red Chalks of the Hunstanton Red Chalk Formation in the Hunstanton and Speeton sections show two peaks at approximately 435 and 570 nm in the FDV patterns, and the value of them decreases but does not completely disappear at 435 nm after heating at 300 °C, suggesting the presence of hematite and a certain amount of clay minerals (Li and Cai, 2014) in addition to a small amount of goethite (Fig. 4); the absence of any characteristic peaks in the white chalks of the Ferriby Chalk Formation suggests the presence of neither hematite nor goethite (Fig. 4a, b). These indicate that there are different types of iron oxides in different strata along the east coast of England. At the same time, the relative content of iron oxides in different strata is also different (Fig. 5). White chalks from the Hunstanton section have a higher goethite/hematite (Gt/Hm) ratio (Fig. 5a). Although Gt/Hm ratios are consistent between sandstone and red chalk, sandstone has the lowest goethite content and red chalk has the highest hematite content (Fig. 5a). In the Speeton section, red chalks have the highest hematite content and the lowest Gt/Hm ratio, while white or gray chalks have the opposite characteristics compared to red chalk (Fig. 5b).

4.3. Trace-element composition

Compilation of trace elements (in ppm) in the samples from the Hunstanton and Speeton sections is presented in Table 1. Compared with trace elements in the upper continental crust (UCC) (Taylor and Mclennan, 1985), the lithophile elements in these samples were

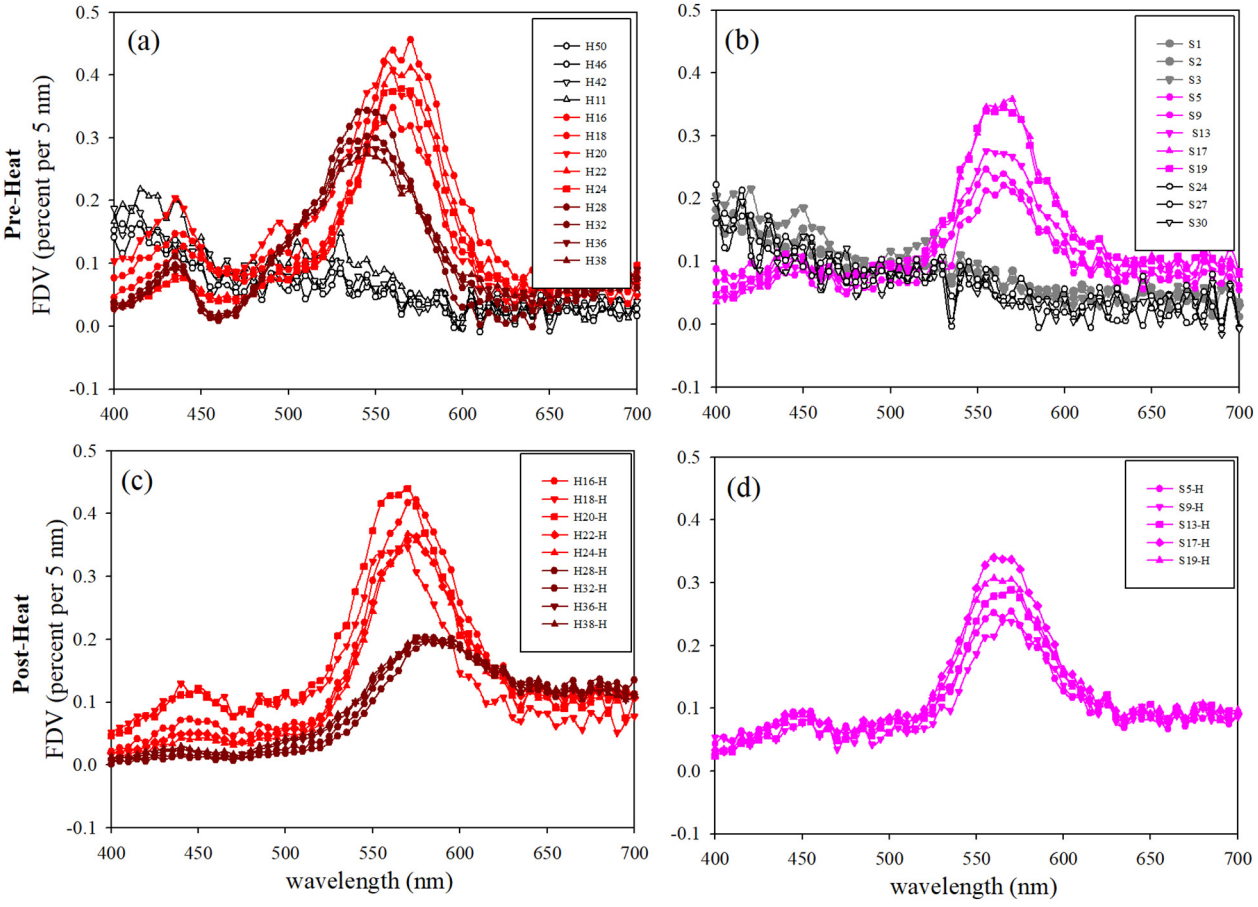

Fig. 4. First derivative spectral patterns of samples before and after heating treatment from Hunstanton (a, c) and Speeton sections (b, d). The sample postfix "-H" means the sample was heated (300 °C, 2 h).

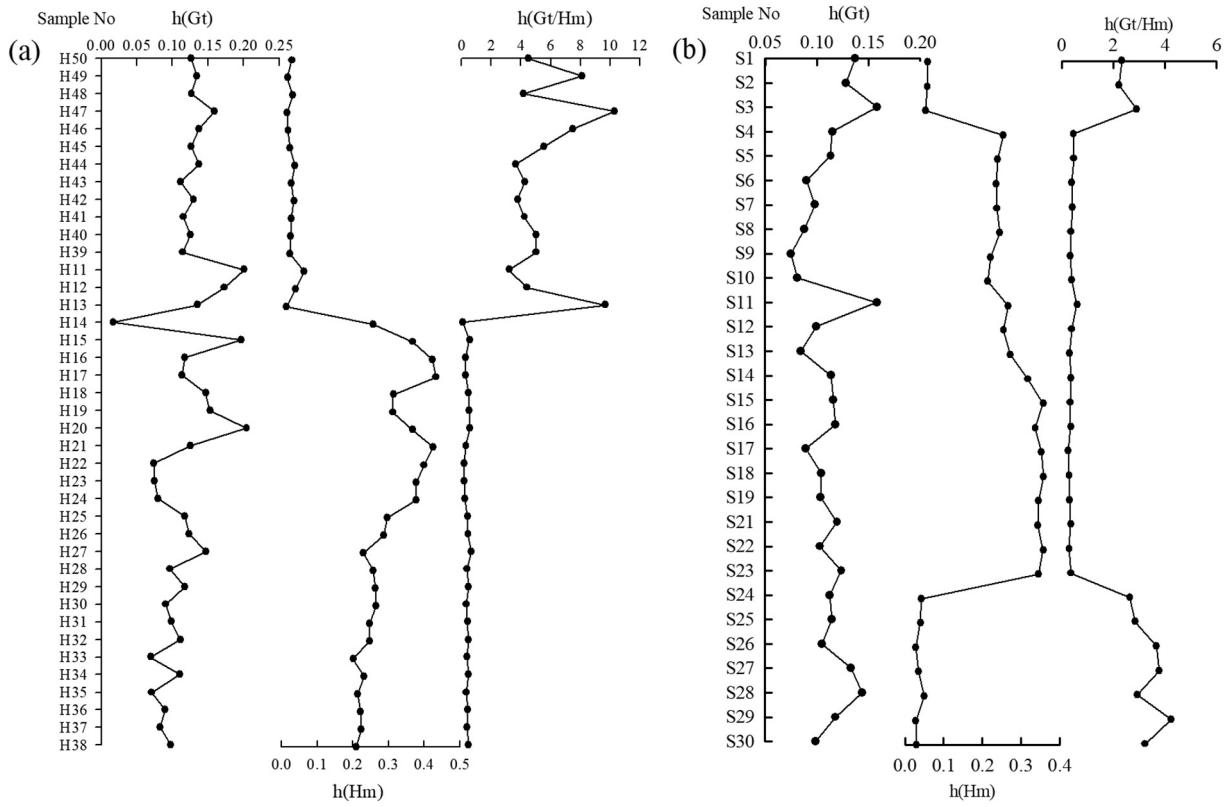

Fig. 5. The relative contents and ratios of hematite and goethite in samples from the Hunstanton (a) and Speeton sections (b). Note: h(Gt) represents the first derivative peak height of diffuse reflectance spectroscopy of goethite. h(Hm) represents the first derivative peak height of diffuse reflectance spectroscopy of hematite. h(Gt/Hm) is the ratio of the first derivative peak height of diffuse reflectance spectroscopy of hematite and goethite.

relatively depleted, such as Ba and Rb, while the sulfurophile elements were relatively enriched, such as As and Cd. The total REE content (ΣREE) of the 11 red chalk samples from the Hunstanton section mainly ranged from 88.3 to 285.93 ppm, with the highest average ΣREE of 188.77 ppm (Table 1), while the lowest average ΣREE of white chalk samples from the Hunstanton section was 58.63 ppm (Table 1). From bottom to top of the Speeton section, the ΣREE of white, red and gray chalks had average values of 165.06 ppm, 146.68 ppm, 131.62 ppm, respectively, which were close to those of the UCC (Table 1). The average ratios of light REEs (LREEs) and heavy REEs (HREEs) in different lithologic samples from the Hunstanton and Speeton sections were 5.84–8.39, which were lower than those in UCC (Table 1). The chondrites normalized REE patterns of samples from the Hunstanton and Speeton sections were mainly characterized by enrichment in LREEs, depletion in HREEs, negative Eu anomaly and positive Gd anomaly, roughly overlapping with those of UCC (Fig. 6a, b, c, d, e) (Taylor and Mclennan, 1985). The calculated average Eu/Eu* ratios of samples from the Hunstanton and Speeton sections ranged from 0.65 to 0.69, almost the same as those in UCC (Table 1). The calculated average Ce/Ce* ratio of samples from the Carstone Formation was 1.28 (Table 1), displaying a positive Ce anomaly, which was different from those from the Hunstanton Red Chalk Formation and Ferriby Chalk Formation. The chondrites normalized REE patterns for shale samples from the Hunstanton section showed distinct bands in three different formations (Fig. 6a, c, e).

4.4. Iron isotope composition

The characteristics of Fe isotopes in sediments are mainly affected by Fe sources, redox conditions and biological processes (Dauphas et al., 2017). For example, Fe isotopes can show large negative values when affected by bacterial Fe oxidation (Préat et al., 2018). Since the most mobile phases in soil are isotopically light, they generally exhibit heavier Fe isotopes than igneous rocks (Beard et al., 2003; Poitrasson et al., 2008; Guelke et al., 2010; Akerman et al., 2014; Li et al., 2017). Therefore, Fe isotopes can allow us to trace Fe cycling and provide favorable insights into the depositional mechanisms. The iron isotopic compositions of 14 representative red chalks from the Hunstanton and Speeton sections are presented in Table 2. The δ^{56}Fe values for the red chalk of the Hunstanton and Speeton sections were mostly positive and ranged from −0.19‰ to 0.12‰ and 0.01‰ to 1.67‰, respectively, with an average of 0.02‰ and 0.38‰, respectively, similar to ferralsol (Poitrasson et al., 2008; Guelke et al., 2010; Akerman et al., 2014; Li et al., 2017) but contrasting that of hydrothermal fluids (Rouxel et al., 2016) and recent organisms (Préat et al., 2018) (Fig. 7).

5. Discussion

5.1. Origin analysis of iron isotope on hematitic pigment

The origin of the hematitic pigment in the Red Chalk Formation in the Middle Cretaceous of Britain has been controversial for a long time. Three hypotheses for hematite in red chalks have been proposed in recent years: diagenetic origin (Jeans, 1973), volcanic or hydrothermal origin (Jeans et al., 2000, 2016) and microbial origin (Andrews et al., 2015). One of the supposed evidences of microbial origin is associated with a questionable microbial structure: *Frutexites*, but this is particularly rare (Jeans, 1980; Andrews et al., 2015). Previously, the identification of microbial origin was mainly based on unique ferruginous morphs, such as stromatolites, filaments, or coccoids (Mamet and Préat, 2006; Préat et al., 2018). The iron isotopic compositions of recent marine organisms and the red facies of the Rosso Ammonitico from the Middle Jurassic were negative and displayed significant Fe isotope variations (Fig. 7). Then, the iron isotopes were used as an additional argument for the activity of the iron bacteria causing the red pigmentation of the samples (Préat et al., 2018). The average δ^{56}Fe values of the red chalk from the Hunstanton and Speeton sections were 0.02‰ and

Table 1
Compilation of trace elements (in ppm) in the samples from the Hunstanton and Speeton sections. The minimum and maximum concentrations of samples of different formations or colors, as well as their average concentrations, are presented in the table. The whole data can be found in the Electronic supplementary materials. (n = number of measurements.)

Element	Hunstanton section									Speeton section									UCC
	White red chalk (n = 15)			Red chalk (n = 11)			Carstone (n = 14)			Gray chalk (n = 3)			Red chalk (n = 18)			White chalk (n = 7)			
	Min.	Max.	Av.	Min.	Max.	Av.	Min.	Max.	Av.	Min.	Max.	Av.	Min.	Max.	Av.	Min.	Max.	Av.	
Sc	1.91	6.01	3.17	5.21	13.83	8.88	9.12	15.65	11.90	5.12	12.84	9.03	4.49	13.67	9.00	4.85	14.23	10.04	11
V	5.27	28.03	11.85	28.95	272.82	112.46	234.00	469.86	340.24	16.41	29.48	24.62	12.07	50.90	28.15	13.76	95.22	42.10	60
Cr	0.00	12.17	3.72	16.18	151.01	61.52	144.84	298.82	204.06	7.34	16.20	11.78	3.77	26.03	12.31	5.18	35.91	18.15	35
Co	1.35	35.97	10.04	3.85	130.53	20.02	15.97	31.68	22.72	7.28	21.80	13.37	4.78	27.26	11.33	2.18	41.08	19.98	10
Ni	7.52	68.31	25.28	41.57	780.02	144.50	87.99	210.80	135.40	22.01	58.06	37.78	16.22	87.25	38.21	6.13	83.14	38.59	20
Cu	2.20	86.13	17.43	5.53	379.65	50.38	4.70	40.68	12.08	8.16	13.48	11.36	2.41	19.42	9.42	11.46	129.06	48.93	25
Zn	0.00	56.13	20.24	22.33	373.80	80.40	78.50	206.19	120.82	7.00	35.33	19.46	1.57	39.41	18.29	0.25	50.64	20.85	71
As	0.83	20.21	5.62	35.88	281.21	105.15	51.41	269.50	126.97	1.32	3.00	2.15	1.44	5.70	3.00	3.43	146.96	45.61	1.5
Rb	2.96	15.67	5.42	8.67	70.45	24.85	23.41	43.57	33.15	10.43	29.14	19.14	11.16	44.56	24.58	7.37	57.88	29.45	112
Sr	473.08	732.79	575.73	140.06	367.27	266.36	41.50	129.82	58.69	498.52	650.52	589.27	474.92	1025.08	663.57	650.14	1506.18	1012.93	350
Y	10.56	42.59	14.86	13.58	113.47	42.72	10.68	37.82	17.89	17.22	35.23	25.01	16.18	34.10	25.52	17.00	40.44	29.88	22
Zr	3.79	28.23	9.70	31.00	200.82	87.82	135.50	262.66	191.16	18.69	46.90	31.14	17.57	95.06	46.15	10.32	79.92	45.33	190
Nb	0.00	2.13	1.01	4.43	32.53	14.90	16.69	51.14	29.30	0.81	4.79	2.42	1.08	19.94	5.43	0.08	9.00	4.48	25
Cd	0.15	1.73	0.40	0.16	0.75	0.46	0.03	0.25	0.11	0.12	0.17	0.15	0.06	0.19	0.14	0.09	0.23	0.14	0.098
Cs	0.09	0.84	0.23	0.38	3.56	1.20	0.98	1.86	1.43	0.48	1.43	0.93	0.49	2.32	1.17	0.55	2.94	1.40	3.7
Ba	11.72	33.54	17.05	31.69	220.04	73.35	88.22	299.64	143.94	32.97	78.56	53.69	32.05	113.56	69.42	27.06	146.88	81.89	550
La	3.34	36.59	13.52	17.07	88.44	41.22	17.80	62.80	28.70	18.27	36.98	26.22	17.44	37.86	29.25	18.19	45.42	32.79	30
Ce	3.62	54.27	16.79	35.02	99.97	63.06	48.30	228.16	84.41	26.20	64.93	43.10	29.21	73.96	52.15	26.31	81.89	55.55	64
Pr	0.70	10.29	3.18	4.35	16.18	9.80	5.65	17.31	8.34	4.26	11.11	7.22	4.27	11.43	7.76	3.99	14.29	9.01	7.1
Nd	2.83	44.20	13.19	17.20	67.50	39.88	21.26	60.49	31.48	17.35	45.70	29.85	17.17	47.57	31.49	15.91	59.29	36.96	26
Sm	0.45	9.64	2.74	3.49	13.08	8.15	4.34	10.88	6.42	3.67	9.70	6.35	3.44	10.54	6.59	3.23	12.59	7.82	4.5
Eu	0.13	2.20	0.63	0.76	3.05	1.80	0.92	2.36	1.31	0.82	2.22	1.44	0.80	2.28	1.47	0.76	2.78	1.76	0.88
Gd	0.62	9.71	2.89	3.38	15.89	8.49	3.87	10.79	5.70	3.70	9.32	6.17	3.49	9.53	6.36	3.41	11.63	7.52	3.8
Tb	0.09	1.30	0.40	0.47	2.11	1.15	0.56	1.43	0.79	0.52	1.31	0.85	0.49	1.22	0.87	0.46	1.56	1.03	0.64
Dy	0.52	7.20	2.30	2.72	13.04	6.54	2.91	8.12	4.29	2.86	7.11	4.67	2.88	6.96	4.84	2.78	8.33	5.70	3.5
Ho	0.10	1.31	0.45	0.51	2.75	1.28	0.54	7.66	0.78	0.57	1.30	0.88	0.54	1.28	0.89	0.55	1.50	1.06	0.8
Er	0.27	3.33	1.25	1.46	8.01	3.59	1.53	8.45	2.23	1.50	3.53	2.37	1.55	3.41	2.45	1.52	3.94	2.87	2.3
Tm	0.03	0.40	0.16	0.21	1.03	0.46	0.24	9.24	0.32	0.19	0.44	0.30	0.21	0.45	0.31	0.20	0.51	0.37	0.33
Yb	0.19	2.24	0.99	1.43	6.24	2.91	1.65	10.04	2.17	1.26	2.83	1.91	1.27	2.95	1.98	1.27	3.13	2.30	2.2
Lu	0.03	0.32	0.14	0.22	0.95	0.43	0.23	10.83	0.32	0.17	0.40	0.27	0.18	0.41	0.28	0.19	0.44	0.33	0.32
Hf	0.06	0.57	0.18	0.65	4.83	2.20	3.90	7.13	5.42	0.46	1.18	0.78	0.44	2.70	1.18	0.25	2.08	1.17	5.8
Pb	2.42	7.57	10.03	5.52	67.33	14.68	12.78	21.79	16.98	6.83	8.91	7.81	6.32	14.47	9.91	5.71	26.61	13.11	20
Th	0.36	2.01	0.76	1.73	11.45	5.16	9.61	19.04	12.81	1.91	4.80	3.26	1.79	5.96	4.06	0.95	8.09	4.41	10.7
U	0.27	4.31	1.16	0.25	1.63	0.72	0.57	1.04	0.74	0.27	0.52	0.39	0.16	0.50	0.34	0.16	1.01	0.56	2.8
La/Th	10.83	28.89	19.94	2.78	51.25	13.95	1.44	4.29	2.25	7.63	9.54	8.29	5.81	10.56	7.74	5.61	19.12	9.75	2.80
La/Sc	1.36	5.94	4.15	2.09	10.88	5.07	1.53	4.48	2.37	2.57	3.57	3.00	2.56	4.05	3.33	2.61	4.08	3.39	2.73
Co/Th	3.66	41.33	12.30	1.42	16.79	3.60	1.25	2.03	1.79	3.59	4.54	3.98	1.39	4.23	2.79	2.60	6.38	4.24	0.93
La/Yb	11.42	17.69	13.55	11.62	16.36	13.88	8.07	31.94	13.32	13.05	14.52	13.97	12.83	17.36	14.86	12.86	15.28	14.26	13.64
LREE/HREE	0.32	2.34	5.84	4.72	8.04	6.60	3.95	21.48	8.39	6.50	6.65	6.56	6.73	7.76	7.16	6.59	7.01	6.79	9.54
∑REE	12.92	100.62	58.63	88.30	285.93	188.77	114.19	398.86	179.82	81.35	196.90	131.62	82.97	201.77	146.68	78.76	247.11	165.06	146.37
δEu	0.63	0.77	0.69	0.63	0.68	0.66	0.59	0.67	0.65	0.68	0.71	0.69	0.58	0.72	0.69	0.68	0.71	0.69	0.69
δCe	0.48	0.66	0.59	0.28	1.03	0.81	0.85	1.64	1.28	0.69	0.76	0.73	0.75	0.93	0.81	0.71	0.79	0.76	0.77

Notes: $\delta Ce = 2Ce_N / (La_N + Pr_N)$, $\delta Eu = 2Eu_N / (Sm_N + Gd_N)$, and the value of chondrite and UCC after Taylor and Mclennan (1985).

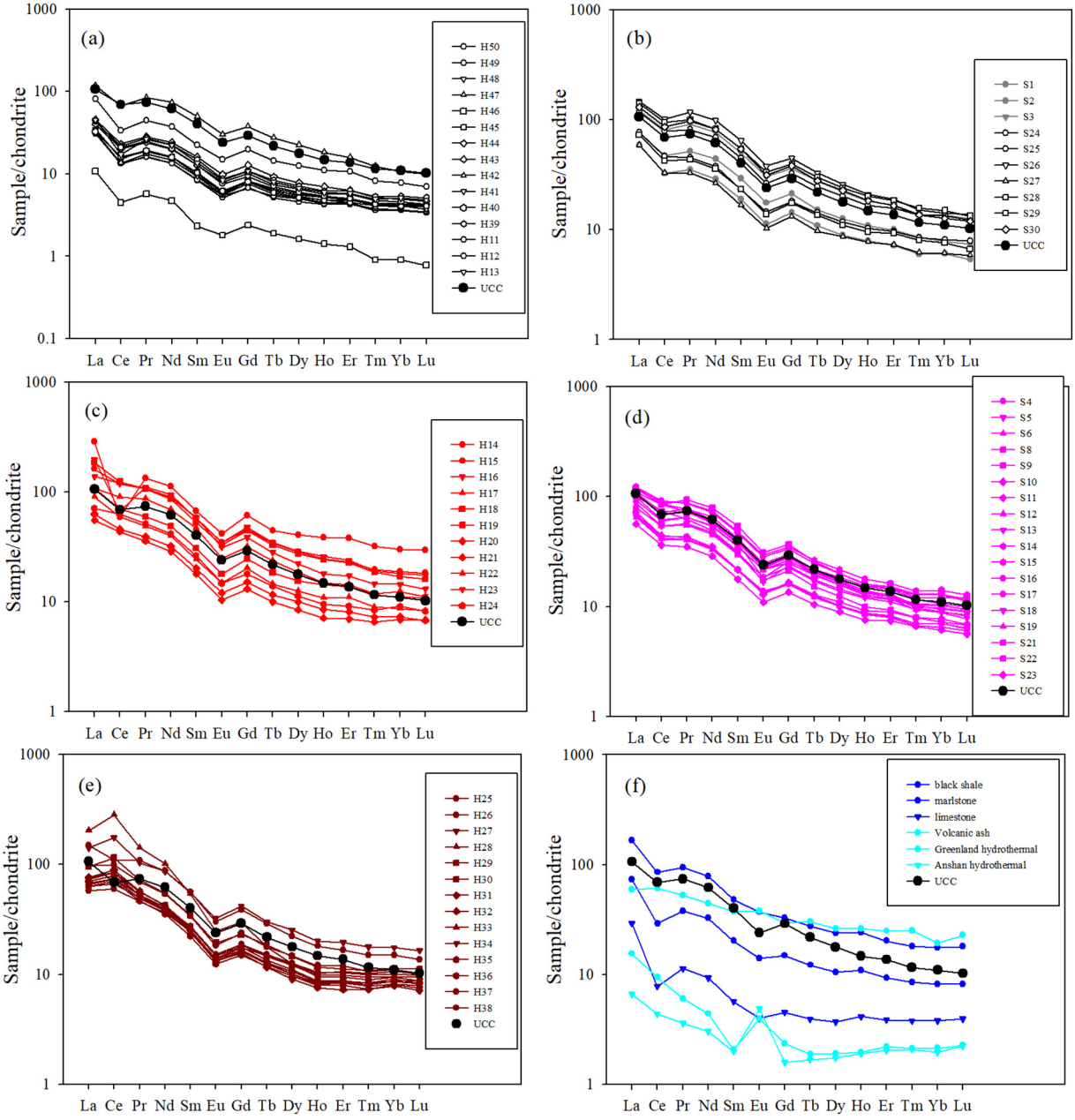

Fig. 6. Rare earth elemental (REE) distribution pattern of samples from the Hunstanton and Speeton sections in the Middle Cretaceous England. (Data from Zhang and Liu (1996), Bellanca et al. (1997), Frei and Polat (2007), and Li et al. (2008).)

Table 2
Fe isotope compositions of the samples from the Hunstanton and Speeton sections.

Sample	δ^{56}Fe (‰)	δ^{57}Fe (‰)	N
H14	0.01 ± 0.05	0.24 ± 0.10	3
H16	−0.19 ± 0.07	−0.31 ± 0.09	3
H18	0.10 ± 0.09	0.15 ± 0.11	3
H20	0.09 ± 0.06	0.18 ± 0.12	3
H22	0.12 ± 0.07	0.16 ± 0.14	3
H24	−0.01 ± 0.08	0.26 ± 0.15	3
S5	0.28 ± 0.06	0.46 ± 0.09	3
S9	0.18 ± 0.05	0.27 ± 0.13	3
S11	0.17 ± 0.07	0.19 ± 0.09	3
S13	0.29 ± 0.06	0.48 ± 0.15	3
S15	0.01 ± 0.08	0.12 ± 0.18	3
S17	0.13 ± 0.06	0.23 ± 0.12	3
S19	0.32 ± 0.07	0.46 ± 0.13	3
S23	1.67 ± 0.08	1.82 ± 0.17	3

0.38‰ (Table 2), respectively, which is consistent with the Fe isotopic signature of the terrestrial baseline derived from igneous and low-Corg clastic sedimentary rocks (Fig. 7) (Beard and Johnson, 2004). The Fe isotopic result does not support the marine biological origin previously proposed.

Evidences of the hydrothermal or volcanic origin of hematite in red chalks have been reviewed in detail (Jeans et al., 2016), which was postulated to be based on the clay mineral assemblages, hematitic pigment and the iron contents of the bioclastic calcite shells from its coeval strata in southern England (Jeans, 1973, 2006; Jeans et al., 2000). One of the most promising applications of iron isotopes has been as important "fingerprints" for determining whether or not they are derived from the hydrothermal fluids in recent years (Dauphas et al., 2017). Recent studies have suggested that hydrothermal Fe at the seafloor may be transported over long distances by chelating into the hydrothermal plumes that form stable organic

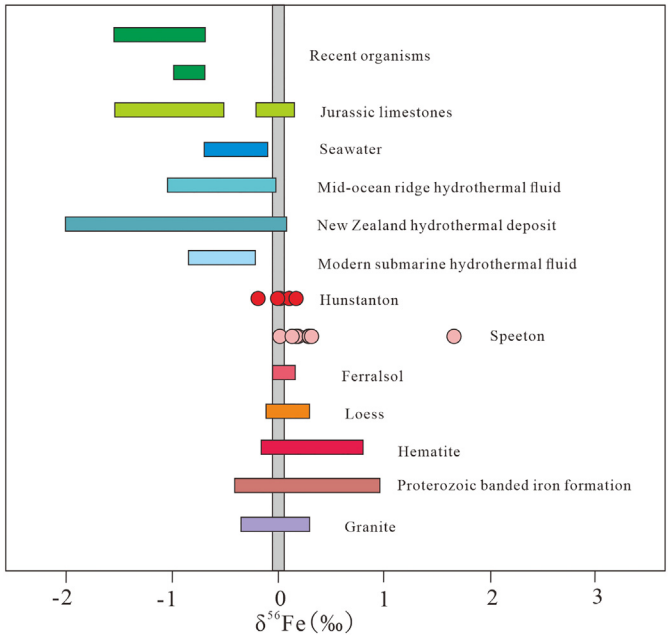

Fig. 7. Iron isotopic distribution in major terrestrial reservoirs and red chalks in the Hunstanton and Speeton sections.
(Modified from references Shi et al. (2018).) (Data from Préat et al. (2018) on Jurassic limestone and recent organisms.) (Data from Poitrasson et al. (2008), Guelke et al. (2010), Akerman et al. (2014), and Li et al. (2017) on ferralsol.) (Data from Beard et al. (2003) on igneous rocks.)

metal chelates (King et al., 1989; Fitzsimmons et al., 2017; Nasemann et al., 2018). The δ^{56}Fe signatures of hydrothermal fluids and hydrothermal sediments at the seafloor are typically lower than those of igneous rocks (Fig. 7) (Beard et al., 2003; Rouxel et al., 2016; Shi et al., 2018). However, most of the red chalks from the Hunstanton and Speeton sections had δ^{56}Fe values in the range from 0.01‰ to 0.32‰ (Table 2), suggesting that the iron in the red chalk may not have originated from seafloor hydrothermal fluids. Except for samples H16 and S23, the red chalk from the Hunstanton and Speeton sections had a narrow range of δ^{56}Fe isotopic compositions, ranging from −0.01‰ to 0.12‰ and 0.01‰ to 0.32‰ (Table 2), respectively, which are similar to the Fe isotopic compositions of ferralsol and loess (Fig. 7) (Beard et al., 2003; Poitrasson et al., 2008; Akerman et al., 2014; Li et al., 2017). This reflects the conservative behavior of Fe during weathering under oxygenated surface conditions (Beard and Johnson, 2004).

5.2. Provenance of non-carbonate components

Trace elements in marine sediments originate from sources including eolian particles, sediments transported by rivers and glaciers, and hydrothermal inputs from mid-ocean ridges (Glasby, 1991; Smrzka et al., 2019). Trace elements on sedimentary rocks play an important role in identifying provenance and determining the tectonic setting of sediments because the rare earth elements (REEs), Th, and Sc are not seriously affected by diagenesis, metamorphism and heavy mineral fractionations (Taylor and Mclennan, 1985; Singh, 2009). The chondrite normalized REE patterns of samples from the Hunstanton and Speeton sections were mainly characterized by enrichment in LREEs, depletion in HREEs, and negative Eu anomaly, roughly overlapping with those of UCC (Fig. 6a, b, c, d, e) (Taylor and Mclennan, 1985), which is contradictory to the positive Eu anomaly of hydrothermal input (Fig. 6f) (Zhang and Liu, 1996; Frei and Polat, 2007; Li et al., 2008; Planavsky et al., 2010). This pattern is also similar to that of the Cretaceous black/marlstone from Venetian region, Italy (Fig. 6f) (Bellanca et al., 1997). Samples from the Hunstanton and Speeton sections have a higher total amount of rare earth elements than the Cretaceous limestone from Venetian region, Italy (Fig. 6f) (Bellanca et al., 1997).

The La/Th–Hf (Floyd and Leveridge, 1987), La/Sc–Co/Th (Gu et al., 2002), La/Yb–ΣREE (Allègre and Minster, 1978), Hf–Co–Th (Savoy et al., 2000) diagrams can further indicate the provenance of the sediments. The discrimination diagram of La/Th–Hf, La/Sc–Co/Th, and Hf–Co–Th is more conclusive in this regard in defining the upper continental crust as a source of non-carbonate components in the red chalks based on samples from the Carstone and Hunstanton Red Formations in the Hunstanton section and from the Hunstanton Red Formation in the Speeton section, which fall into the region of felsic protolith and andesitic protolith, respectively (Fig. 8a, b, d). Moreover, the La/Yb vs. ΣREE diagram further indicates its geochemical similarity to sedimentary rocks with a small amount of granite (Fig. 8c) (Allègre and Minster, 1978). It follows that most of non-carbonate components of the red chalk derived from the felsic rocks and sedimentary derivatives without mantle material input.

5.3. Evidence of pedogenic modification

A detrital origin is when hematite was derived from continental weathering during sedimentation (Von Houten, 1961; Zhang, 2015). Since the clay mineral assemblages of the red chalk are different from those of the Triassic or Devonian red beds, a new origin, that is the diagenetic origin, of hematitic pigment in the red chalk has been proposed (Jeans, 1973). Red chalks in the Hunstanton section are co-stained with hematite and a small amount of goethite (Fig. 4a, c), which was formed in an arid, oxidized environment (Liu et al., 2014; Gao et al., 2018) that was typical of the greenhouse climate of the mid-Cretaceous period (Tierney et al., 2020). Rubification of iron hydroxides proceeds in a few tens of thousands of years when soils are buried to form sedimentary rocks (Retallack, 2001). The presence of goethite since the Cretaceous indicates that the hematite in the red chalk was formed in a synsedimentary oxidation environment, rather than the formation of iron hydroxide dehydration in the later diagenetic stage because it had been affected by hard-ground development (Walker, 1967; Jeans, 1973).

Previous studies have shown that red beds formed in the underwater environment are characterized by homogeneous strata, such as Cretaceous oceanic red beds (X.M. Hu et al., 2012). The coexistence of red and white appears in the soil-forming environment, such as vertisols and vermicular red earth (Soil Survey Staff., 2014). However, the hematite of the Hunstanton Red Chalk Formation is distributed in the chalk matrix with a reticulate form (Figs. 2d, e, 3b, d), which indicates that the sedimentary environment is not permanently underwater. The recognition of paleosols is characterized by traces of life, soil horizons and soil structure (Retallack, 2001). Mudcracks are caused by shrinkage cracking during periods of emergence and are very weakly developed, typically under sub-humid to semiarid conditions (Armenteros et al., 1997). At the top of the Hunstanton Red Chalk Formation, the mudcracks of the red chalk are filled with either red or white chalk (Fig. 2h). Calcicretes or calcareous nodules are a product of soil formation, which are formed by the dissolution of carbonate in the subsoil and the carbonate precipitation near the soil surface due to changes in the amount of water by evaporation or the decrease of CO_2 concentration (Li et al., 2018; Valera-Fernández et al., 2020; Menezes et al., 2021). Calcareous or calcareous nodules are difficult to recognize in karstic coastal environments, so they can be easily considered as irrelevant to pedogenic processes (Alonso-Zarza and Wright, 2010). The bottom of the overlying white Ferriby Chalk Formation contains a large number of morphologically diverse calcareous nodules (Fig. 2c). Secondary white chalks in the Speeton section are formed at inclined or vertical fractures of the red chalk formation (Fig. 2b, f).

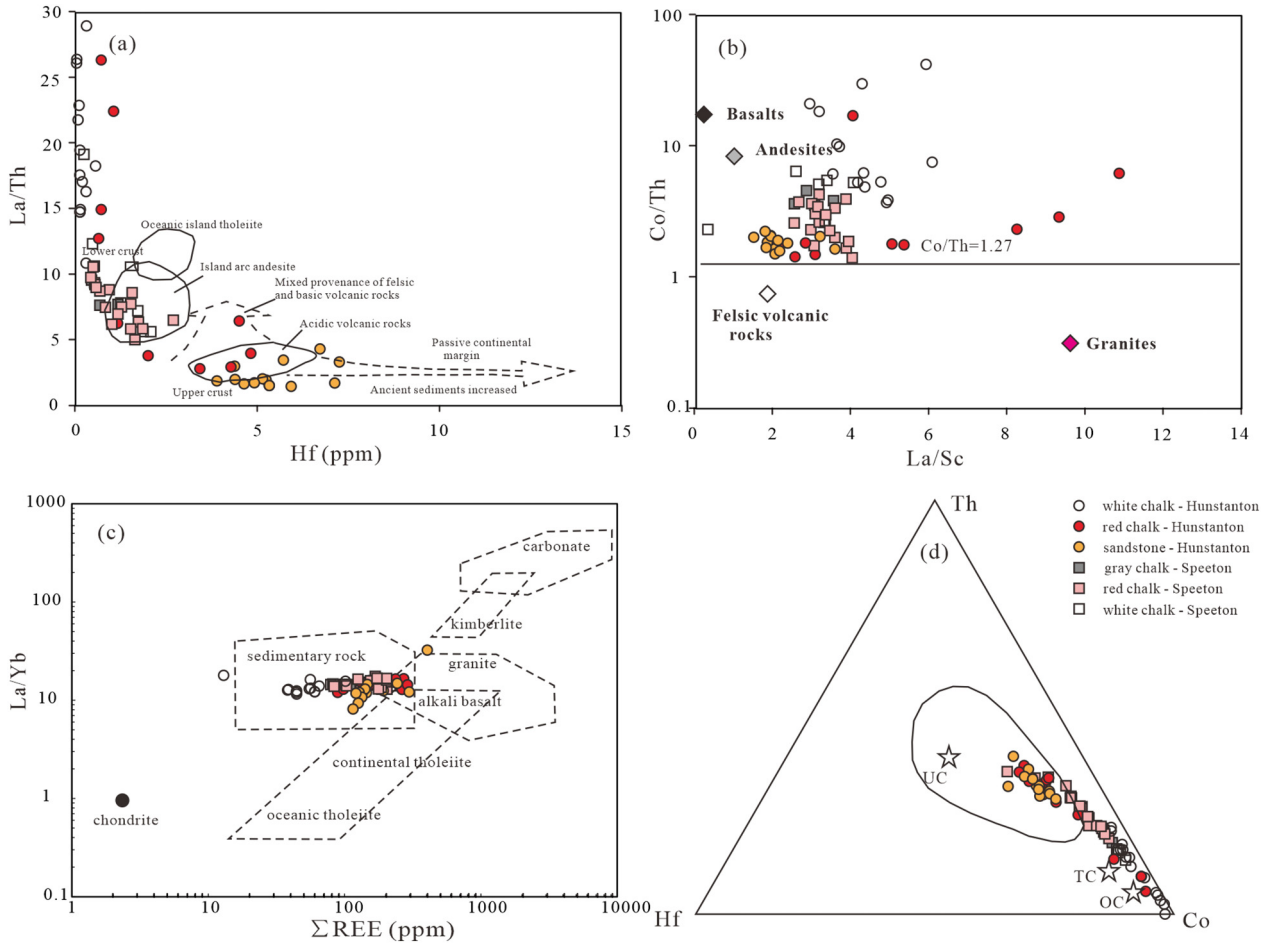

Fig. 8. The source rocks discrimination diagrams about La/Th–Hf (a), La/Sc–Co/Th (b), La/Yb–ΣREE (c) and Hf–Co–Th (d) for samples from the Hunstanton and Speeton sections. (After Allègre and Minster (1978), Floyd and Leveridge (1987), Savoy et al. (2000), and Gu et al. (2002).)

Although the relative hematite and goethite contents of the secondary white chalks are similar to those of the white chalk in the Hunstanton section (Fig. 5), the ΣREE of the secondary white chalk is consistent with that of the red chalk in the Speeton section, but higher than that of the White chalk in the Hunstanton section (Table 2), indicating that the secondary white chalks were formed later than the red chalks (Fig. 2f). Such a phenomenon is caused by the dissolution and loss of Fe^{3+} in a moist environment, and then illuviation in an arid environment (Schaetzl and Anderson, 2005). The iron bearing mineral of the underlying brown pebbly sandstone of the Carstone Formation in the Hunstanton section is goethite (Fig. 4a, c), which was formed in a humid oxidizing environment (Liu et al., 2014). This is also supported by previous studies that determined that the Carstone Formation was formed within a relatively shallow water environment that is conducive to the formation of goethite (Owen, 1995). All the above phenomena and the sedimentary environment of the overlying and underlying strata suggest that the pedogenic origin is indisputable. Therefore, it is inferred that the red chalk was deposited in the supratidal environment that had undergone some degree of desiccation and pedogenic modification before the global transgression of the Cretaceous (Belghouthi et al., 2019).

6. Conclusions

Red chalks are an enigmatic feature of the Cretaceous Chalk in eastern England. The evidence gathered through diffuse reflection, trace element and iron isotope analysis and combining with the lithologic and stratigraphic characteristics led to the following conclusions:

(1) The Fe isotopic composition and negative Eu anomaly indicate that the Fe sources and origin of hematite in the red chalks are not of marine microbial or hydrothermal, but of sedimentary origin.
(2) The chondrite normalized REE patterns, La/Th–Hf, La/Sc–Co/Th, La/Yb–ΣREE, and Hf–Co–Th diagrams indicate the felsic rocks and sedimentary derivatives as a source of non-carbonate components in the red chalks.
(3) Mudcracks and secondary white chalks appear in the red chalks, as well as the overlying white Ferriby Chalk Formation with a large number of calcareous nodules and the underlying Carstone formation composed of pebbly sandstone, indicating that the hematite of the red chalks is of pedogenic origin. Therefore, it is inferred that the red chalk was deposited in the supratidal environment that had undergone some degree of desiccation and pedogenic modification.

Declaration of competing interest

No conflict of interest exists in the submission of this manuscript, and the manuscript is approved by all authors for publication. I would like to declare on behalf of my co-authors that the work described was original research that has not been published previously, and not under consideration for publication elsewhere, in whole or in part. All the authors listed have approved the manuscript.

Acknowledgments

This work was supported by National Natural Science Foundation of China (41772180, 41210002). We would like to express our gratitude to Yifei Fan for helping in the experiment of trace elements. Then, constructive comments from two anonymous reviewers and manuscript handling by the editor Dr. Catherine Chagué are highly appreciated.

Appendix A. Supplementary data

Supplementary data to this article can be found online at https://doi.org/10.1016/j.sedgeo.2021.106073.

References

Akerman, A., Poitrasson, F., Oliva, P., Audry, S., Prunier, J., Braun, J.J., 2014. The isotopic fingerprint of Fe cycling in an equatorial soil–plant–water system: the Nsimi watershed, South Cameroon. Chemical Geology 385, 104–116.
Aliyu, M.M., 2016. The Origin and Properties of Flint in the Upper Cretaceous Chalk. The University of Leeds, Leeds (Ph.D. thesis, 283 pp.).
Allègre, C.J., Minster, J., 1978. Quantitative models of trace element behavior in magmatic processes. Earth and Planetary Science Letters 1, 1–25.
Alonso-Zarza, A.M., Wright, V.P., 2010. Calcretes. In: Alonso-Zarza, A.M., Tanner, L.H. (Eds.), Carbonates in Continental Settings. Developments in Sedimentology. Elsevier, pp. 117–224.
Andrews, J.E., Kendall, A.C., Hall, A., 2015. Microbial crust with Frutexites(?) and iron staining in chalks: Albian–Cenomanian boundary, Hunstanton, UK. Geological Magazine 1, 1–11.
Armenteros, I., Daley, B., Garcia, E., 1997. Lacustrine and palustrine facies in the Bembridge Limestone (late Eocene, Hampshire Basin) of the Isle of Wight, southern England. Palaeogeography, Palaeoclimatology, Palaeoecology 128, 111–132.
Balsam, W.L., Ji, J.F., Renock, D., Deaton, B.C., Williams, E.R., 2014. Determining hematite content from NUV/Vis/NIR spectra: limits of detection. American Mineralogist 11-12, 2280–2291.
Beard, B.L., Johnson, C.M., 2004. Fe isotope variations in the modern and ancient earth and other planetary bodies. Reviews in Mineralogy and Geochemistry 1, 319–357.
Beard, B.L., Johnson, C.M., Skulan, J.L., Nealson, K.H., Cox, L., Sun, H., 2003. Application of Fe isotopes to tracing the geochemical and biological cycling of Fe. Chemical Geology 195, 87–117.
Belghouthi, F., Zouari, H., Jeddi, R.S., 2019. The lower Maastrichtian chalk in the Ghezala–Mateur area, northern Tunisian domain: sedimentary environments and early diagenetic features. Journal of African Earth Sciences 149, 291–306.
Bellanca, A., Masetti, D., Neri, R., 1997. Rare earth elements in limestone/marlstone couplets from the Albian–Cenomanian Cismon section (Venetian region, northern Italy): assessing REE sensitivity to environmental changes. Chemical Geology 141, 141–152.
Cai, Y.F., Hu, X.X., Li, X., Pan, Y.G., 2012. Origin of the red color in a red limestone from the Vispi Quarry section (central Italy): a high-resolution transmission electron microscopy analysis. Cretaceous Research 38, 97–102.
Craddock, P.R., Dauphas, N., 2011. Iron isotopic compositions of geological reference materials and chondrites. Geostandards and Geoanalytical Research 1, 101–123.
Dauphas, N., John, S.G., Rouxel, O., 2017. Iron isotope systematics. Reviews in Mineralogy and Geochemistry 1, 415–510.
Fitzsimmons, J.N., John, S.G., Marsay, C.M., Hoffman, C.L., Nicholas, S.L., Toner, B.M., German, C.M., Sherrell, R.M., 2017. Iron persistence in a distal hydrothermal plume supported by dissolved-particulate exchange. Nature Geoscience 10, 195–201.
Floyd, P.A., Leveridge, B.E., 1987. Tectonic environment of the Devonian Gramscatho basin, south Cornwall: framework mode and geochemical evidence from turbiditic sandstones. Journal of the Geological Society 144, 531–542.
Frei, R., Polat, A., 2007. Source heterogeneity for the major components of ~3.7Ga Banded Iron Formations (Isua Greenstone Belt, Western Greenland): tracing the nature of interacting water masses in BIF formation. Earth and Planetary Science Letters 1-2, 266–281.
Gao, X.B., Hao, Q.Z., Wang, L., Oldfield, F., Bloemendal, J., Deng, C.L., Song, Y., Ge, J.Y., Wu, H. B., Xu, B., Li, F.J., Han, L., Fu, Y., Guo, Z.T., 2018. The different climatic response of pedogenic hematite and ferrimagnetic minerals: evidence from particle-sized modern soils over the Chinese Loess Plateau. Quaternary Science Reviews 179, 69–86.
Giorgioni, M., Weissert, H., Bernasconi, S.M., Hochuli, P.A., Keller, E.C., Coccioni, R., Petrizzo, M.R., Lukeneder, A., Garcia, T.I., 2015. Paleoceanographic changes during the Albian–Cenomanian in the Tethys and North Atlantic and the onset of the Cretaceous chalk. Global and Planetary Change 126, 46–61.
Glasby, G.P., 1991. Mineralogy, geochemistry, and origin of Pacific red clays: a review. New Zealand Journal of Geology and Geophysics 34, 167–176.
Gu, X.X., Liu, J.M., Zheng, M.H., Tang, J.X., Qi, L., 2002. Provenance and tectonic setting of the Proterozoic turbidites in Hunan, South China: geochemical evidence. Journal of Sedimentary Research 72, 393–407.
Guelke, M., Blanckenburg, F.V., Schoenberg, R., Staubwasser, M., Stuetzel, H., 2010. Determining the stable Fe isotope signature of plant-available iron in soils. Chemical Geology 3-4, 269–280.
Guo, X.L., Retallack, G.J., Lü, B., He, L.S., Wang, R.H., Song, H., 2018. Paleosols in Devonian red-beds from Northwest China and their paleoclimatic characteristics. Sedimentary Geology 379, 16–24.
Hancock, J.M., 1975. The petrology of the Chalk. Proceedings of the Geologists Association 4, 499–535.
Hopson, P.M., Wilkinson, I.P., Woods, M.A., 2008. A stratigraphical framework for the Lower Cretaceous of England. British Geological Survey Research Reports RR/08/03 (British, 77 pp.).
Hu, X.F., Jeans, C.V., Dickson, T., 2012a. Geochemical and stable isotope patterns of calcite cementation in the Upper Cretaceous Chalk, UK: direct evidence from calcite-filled vugs in brachiopods. Acta Geologica Polonica 2, 143–172.
Hu, X.M., Scott, R.W., Cai, Y.F., Wang, C.S., Melinte-Dobrinescu, M.C., 2012b. Cretaceous oceanic red beds (CORBs): different time scales and models of origin. Earth-Science Reviews 115, 217–248.
Jeans, C.V., 1973. The Market Weighton structure: tectonics, sedimentation and diagenesis during the Cretaceous. Proceedings of the Yorkshire Geological Society 3, 409–444.
Jeans, C.V., 1980. Early submarine lithification in the Red Chalk and Lower Chalk of Eastern England: a bacterial control model and its implications. Proceedings of the Yorkshire Geological Society 6, 81–157.
Jeans, C.V., 2006. Clay mineralogy of the Cretaceous strata of the British Isles. Clay Minerals 1, 47–150.
Jeans, C.V., Wray, D.S., Merriman, R.J., Fisher, M.J., 2000. Volcanogenic clays in Jurassic and Cretaceous strata of England and the North Sea Basin. Clay Minerals 1, 25–55.
Jeans, C.V., Turchyn, A.V., Hu, X.F., 2016. Sulfur isotope patterns of iron sulfide and barite nodules in the Upper Cretaceous Chalk of England and their regional significance in the origin of coloured chalks. Acta Geologica Polonica 2, 227–256.
King, C., Bailey, H.W., Burton, C., King, A.D., 1989. Cretaceous of the North Sea, stratigraphical atlas of fossil foraminifera. The British Micropalaeontological Society Series, 2nd edition Ellis Horwood Ltd, Chichester, pp. 372–417.
Lasseur, E., Guillocheau, F., Robin, C., Hanot, F., Vaslet, D., Coueffe, R., Neraudeau, D., 2009. A relative water-depth model for the Normandy Chalk (Cenomanian–Middle Coniacian, Paris Basin, France) based on facies patterns of metre-scale cycles. Sedimentary Geology 213, 1–26.
Li, X., Cai, Y.F., 2014. The colouration mechanism and genetic study of Cretaceous oceanic red beds. Acta Mieralogica Sinica 4, 451–460 (in Chinese with English abstract).
Li, Z.H., Zhu, X.K., Tang, S.H., 2008. Characters of Fe isotope and rare earth elements of banded iron formations from Anshan–Benxi area: implications for Fe source. Acta Petrologica ET Mineraloogica 4, 285–290 (in Chinese with English abstract).
Li, M., He, Y.S., Kang, J.T., Yang, X.Y., He, Z.W., Yu, H.M., Huang, F., 2017. Why was iron lost without significant isotope fractionation during the lateritic process in tropical environments? Geoderma 290, 1–9.
Li, Y.R., Zhang, W.W., Aydin, A., Deng, X.H., 2018. Formation of calcareous nodules in loess–paleosol sequences: reviews of existing models with a proposed new "per evapotranspiration model". Journal of Asian Earth Sciences 154, 8–16.
Liu, X.M., Lü, B., Mao, X.G., Wen, C.H., Yu, M.T., Guo, X.L., Chen, J.S., Wang, T., 2014. Iron minerals of aeolian deposits vary with environment and its significances. Quaternary Sciences 3, 443–457 (in Chinese with English abstract).
Mamet, B., Préat, A.R., 2006. Iron-bacterial mediation in Phanerozoic red limestones: state of the art. Sedimentary Geology 3-4, 147–157.
Menezes, M.N., Dal' Bo, P.F., Smith, J.J., Rodriguesl, A.G., 2021. The influence of ancient soil biota on the precipitation and distribution of pedogenic carbonate in paleosols of the Marília Formation (Upper Cretaceous, Brazil). Palaeogeography Palaeoclimatology Palaeoecology 571, 110375. https://doi.org/10.1016/j.palaeo.2021.110375.
Mitchell, S.F., 1995. Lithostratigraphy and biostratigraphy of the Hunstanton Formation (Red Chalk, Cretaceous) succession at Speeton, North Yorkshire, England. Proceedings of the Yorkshire Geological Society 4, 285–303.
Mortimore, R.N., 2001. Chalk: a stratigraphy for all reasons. Proceedings. Ussher Society 2, 105–122.
Nasemann, P., Gault-Ringold, M., Stirling, C.H., Koschinsky, A., Sander, S.G., 2018. Processes affecting the isotopic composition of dissolved iron in hydrothermal plumes: a case study from the Vanuatu back-arc. Chemical Geology 476, 70–84.
Owen, H.G., 1995. The upper part of the Carstone and the Hunstanton Red Chalk (Albian) of the Hunstanton Cliff, Norfolk. Proceedings of the Geologists' Association 3, 171–181.
Planavsky, N., Bekker, A., Rouxel, O.J., Kamber, B., Hofmann, A., Knudsen, A., Lyons, T.W., 2010. Rare Earth Element and yttrium compositions of Archean and Paleoproterozoic Fe formations revisited: new perspectives on the significance and mechanisms of deposition. Geochimica et Cosmochimica Acta 22, 6387–6405.
Poitrasson, F., Viers, J., Martin, F., Braun, J.J., 2008. Limited iron isotope variations in recent lateritic soils from Nsimi, Cameroon: implications for the global Fe geochemical cycle. Chemical Geology 1-2, 54–63.
Préat, A.R., Ridder, C.D., Gillan, D., 2018. Bacterial origin of the red pigmentation of Phanerozoic carbonate rocks: an integrated study of geology–biology–chemistry. Geologica Belgica 3-4, 167–175.
Price, G.D., 1998. Isotopic variation in fossils and matrix of the Cretaceous Red Chalk at Speeton and South Ferriby, Yorkshire, England. Proceedings of the Yorkshire Geological Society 1, 107–112.
Price, G.D., Harwood, E., 2012. Isotopic analysis of belemnites and brachiopods from the Cretaceous (Albian) Hunstanton Red Chalk Formation (Hunstanton, Norfolk, UK). Proceedings of the Geologists Association 3, 479–485.
Retallack, G.J., 2001. Soils of the Past: An Introduction to Paleopedology. Blackwell Science (404 pp.).
Rouxel, O., Toner, B.M., Manganini, S.J., German, C.R., 2016. Geochemistry and iron isotope systematics of hydrothermal plume fall-out at East Pacific Rise 9 degrees 50′N. Chemical Geology 441, 212–234.
Savoy, L.E., Stevenson, R.K., Mountjoy, E.W., 2000. Provenance of Upper Devonian–Lower Carboniferous miogeoclinal strata, Southeastern Canadian Cordillera: link between tectonics and sedimentation. Journal of Sedimentary Research 70, 181–193.

Schaetzl, R.J., Anderson, S., 2005. Soils: Genesis and Geomorphology. Cambridge University Press, New York (817 pp.).
Shi, T.Q., Xu, H., Zhang, H.Y., Li, X.P., Zhang, W.W., 2018. Research status of Fe isotopes and its application to ferrodolomite study in Xisha Islands. Marine Geology Frontiers 6, 50–55 (in Chinese with English abstract).
Singh, P., 2009. Major, trace and REE geochemistry of the Ganga River sediments: influence of provenance and sedimentary processes. Chemical Geology 266, 242–255.
Smrzka, D., Zwicker, J., Bach, W., Feng, D., Himmler, T., Chen, D., Peckmann, J., 2019. The behavior of trace elements in seawater, sedimentary pore water, and their incorporation into carbonate minerals: a review. Facies 65.
Soil Survey Staff, 2014. Illustrated Guide to Soil Taxonomy. United States Department of Agriculture Natural Resources Conservation Service, National Soil Survey Center, Lincoln, Nebraska (360 pp.).
Surlyk, F., 1997. A cool water carbonate ramp with bryozoan mounds: Late Cretaceous—Danian of the Danish Basin. In: James, N.P., Clarke, J.A.D. (Eds.), Cool-water Carbonates. Special Publicationvol. 56. Society of Economic Paleontologists and Mineralogists, pp. 293–308.
Taylor, S.R., Mclennan, S.M., 1985. The continental crust: its composition and evolution. Journal of Geology 4, 632–633.
Tierney, J.E., Poulsen, C.J., Montañez, I.P., Bhattacharya, T., Feng, R., Ford, H.L., Hönisch, B., Inglis, G.N., Petersen, S.V., Sagoo, N., Tabor, C.R., Thirumalai, K., Zhu, J., Burls, N.J., Foster, G.L., Goddéris, Y., Huber, B.T., Ivany, L.C., Turner, S.K., Lunt, D.J., McElwain, J.C., Mills, B.J.W., Otto-Bliesner, B.L., Ridgwell, A., Zhang, Y.G., 2020. Past climates inform our future. Science 370, 1–9.
Valera-Fernández, D., Cabadas-Báez, H., Solleiro-Rebolledo, E., Landa-Arreguín, F.J., Sedov, S., 2020. Pedogenic carbonate crusts (calcretes) in karstic landscapes as archives for paleoenvironmental reconstructions-a case study from Yucatan Peninsula, Mexico. Catena 194, 104635. https://doi.org/10.1016/j.catena.2020.104635.
Von Houten, F.B., 1961. Climatic significance of red beds. In: Narin, A.E.M. (Ed.), Descriptive Paleoclimatology. Wiley (Interscience), New York, pp. 89–139.
Walker, T.R., 1967. Formation of red beds in modern and ancient deserts. Geological Society of America Bulletin 3, 353–368.
Wang, R., Shi, W.Z., Xie, X.Y., Wang, L.L., Busbey, A.B., Manger, W., Xia, Z.M., 2017. Hydrothermal indications of Early Cretaceous red beds in lacustrine successions, North Yellow Sea Basin, eastern China. Marine and Petroleum Geology 88, 739–755.
Wray, D.S., Gale, A.S., 2006. The palaeoenvironment and stratigraphy of Late Cretaceous Chalks. Proceedings of the Geologists Association 117, 145–162.
Zhabin, A.V., Belyavtseva, E.E., Sirotin, V.I., Mahfuz, Z.H., 2018. New ideas on the origin of chalk in Upper Cretaceous rocks of the Voronezh Anteclise. Doklady Earth Sciences 1, 573–574.
Zhang, X.L., 2015. The Comparison Studies on Three Silurian Red Beds From Yangtze Region, South China and Discussion on Controlling Factors of Clastic Red Beds. Nanjing Institute of Geology and Palaeontology, Chinese Academy of Science, Nanjing (Ph.D. thesis, 190 pp.).
Zhang, W.H., Liu, J.Q., 1996. The composition of volcanic ash from ice core of Collins Cap, King George island of Antarctica. Acta Petrologica Sinica 3, 434–445 (in Chinese with English abstract).
Zhou, W., Ji, J.F., Balsam, W., Chen, J., 2007. Determination of goethite and hematite in red clay by diffuse reflectance spectroscopy. Geological Journal of China Universities 4, 730–736 (in Chinese with English abstract).